Longitudinal changes in white matter free water in cerebral small vessel disease: Relationship to cerebral blood flow and white matter fiber alterations

Miao Lin[1], Shuyue Wang[1], Hui Hong[1], Yao Zhang[1], Linyun Xie[1],
Lei Cui[1], Lingyun Liu[1], Yeerfan Jiaerken[1], Xinfeng Yu[1],
Minming Zhang[1] (iD), Alberto De Luca[2,3], Ruiting Zhang[1] and
Peiyu Huang[1] (iD)

Abstract
White matter (WM) free water (FW) is a potential imaging marker for cerebral small vessel disease (CSVD). This study aimed to characterize longitudinal changes in WM FW and investigate factors contributing to its elevation in CSVD. We included 80 CSVD patients and 40 normal controls (NCs) with multi-modality MRI data. Cerebral blood flow (CBF) was measured, and fiber alterations were assessed using total apparent fiber density (AFD_t). FW were extracted from whole WM, white matter hyperintensities (WMH) and normal-appearing WM (NAWM). Baseline and longitudinal FW elevation were compared between patients and NCs, and between WMH and NAWM. We investigated whether baseline vascular risk factor score, CBF, and AFD_t could predict longitudinal FW elevation. Association between cognition and WM FW in CSVD was also assessed. Results shown that FW was higher and increased faster in CSVD compared to NCs and in WMH compared to NAWM. Baseline AFD_t predicted longitudinal FW elevation in CSVD patients, while CBF predicted FW changes only in controls. WM FW was associated with cognitive impairment. These findings suggest that CSVD is associated with a faster increase in WM FW. Hypoperfusion and WM fiber alterations might accelerate FW elevation, which is associated with cognitive decline.

Keywords
Cerebral small vessel disease, white matter, free water, diffusion-tensor imaging, cerebral blood flow

Introduction

Cerebral small vessel disease (CSVD) is a significant contributor to stroke and dementia.[1] Efforts have been deployed to develop biomarkers for CSVD to improve its' early identification, staging, and prediction of future clinical outcomes.[2,3]

MRI is the method of choice for diagnosing CSVD and monitoring disease progression.[4,5] While conventional MRI hallmarks of CSVD such as white matter hyperintensities (WMH) and lacunes of presumed vascular origin were widely used,[6] recent work converges on the high potential of diffusion imaging metrics as markers for CSVD.[4] Diffusion metrics typically outperform conventional CSVD imaging markers in

[1]Department of Radiology, The 2nd Affiliated Hospital, Zhejiang University School of Medicine, Hangzhou, China
[2]Department of Neurology and Neurosurgery, UMC Utrecht Brain Center, University Medical Center Utrecht, Utrecht, The Netherlands
[3]Image Sciences Institute, University Medical Center Utrecht, Utrecht University, Utrecht, The Netherlands

Corresponding authors:
Peiyu Huang, Department of Radiology, The 2nd Affiliated Hospital, Zhejiang University School of Medicine, No. 88 Jiefang Road, Shangcheng District, Hangzhou 310009, China.
Email: huangpy@zju.edu.cn

Ruiting Zhang, Department of Radiology, The 2nd Affiliated Hospital, Zhejiang University School of Medicine, No. 88 Jiefang Road, Shangcheng District, Hangzhou 310009, China.
Email: zhangruiting@zju.edu.cn

explaining clinical deficits and in detecting disease progression, while also enabling a high grade of automation.[4,7]

Recently, white matter (WM) free water (FW), which reflects the amount of extracellular water content in the WM tissue,[8] demonstrated high potential as a CSVD imaging marker. FW has been found associated with vascular risk factors,[9,10] disease burden assessed by common CSVD imaging markers,[11] and clinical functions.[12,13] The test-retest repeatability and inter-scanner reproducibility were proved excellent in the multi-center MarkVCID study.[7]

Nonetheless, most previous studies were cross-sectional studies, or focused on using baseline FW to predict future clinical outcomes. The longitudinal change of FW in CSVD has not been fully characterized and the driving factors of increased FW are still uncertain. Specifically, it is unknown whether some core CSVD-related features, such as risk factors, vascular changes (hypoperfusion), and WM fiber alterations, could cause the longitudinal increase in FW. Confirming these relationships is crucial for using FW as an imaging marker of CSVD.

In the present study, we used longitudinal multi-modal imaging data from both CSVD patients and normal controls to investigate these questions. We aimed to (1) characterize the longitudinal change of WM FW in CSVD patients versus normal controls, (2) explore whether vascular risk factors, hypoperfusion, and WM fiber alterations would accelerate FW increase, and (3) verify the correlation between FW and cognition.

Materials and methods

Participants

The CSVD cohort. We retrospectively reviewed the data from CSVD patients (defined as the presence of lacunes and/or WMH on MRI) admitted to the neurology department of our hospital from January 2014 to December 2022. Patients were referred to the hospital primarily for acute conditions (e.g., transient ischemic attack and stroke presenting with lacunar syndrome) or subacute symptoms of CSVD (e.g., vascular cognitive impairment and/or gait disturbances). The first MRI scan of patients diagnosed with acute lacunar infarct was acquired at least six months after stroke onset. Subsequent MRI scans were performed annually during the follow-up. All patients received cognitive function assessments based on the Montreal Cognitive Assessment (MoCA) at each visit.

The inclusion criteria were (1) baseline age >40; (2) baseline WMH total score (summing the periventricular and deep WMH Fazekas scores[14]) >1; (3) had at least one follow-up MRI scan; and (4) with complete multi-modality MRI data (including 3 D-T1-weighted (3 D-T1w) images, T2 fluid-attenuated inversion recovery (FLAIR) images, diffusion tenser images) at baseline and follow-up. The exclusion criteria were (1) patients with history of stroke (except for lacunar stroke), brain trauma, neurological or psychiatric diseases, or systemic diseases that could severely affect the brain and interfering with the study design, (2) poor image quality or imaging processing error.

Initially, 93 CSVD patients fulfilled the inclusion criteria. Then, two patients were excluded due to cerebral hemorrhage at follow-up, six patients due to poor T1 or FLAIR images quality, five patients due to technical issues during WMH segmentation. Finally, 80 patients were included for further analyses.

The normal control (NC) cohort. We retrospectively reviewed prospectively collected data from community volunteers recruited by online advertisements and posters. The purpose of recruit was to construct a control group for our clinical brain imaging study. The inclusion criteria were (1) age >40; (2) had at least one follow-up MRI scans; and (3) with complete multi-modality MRI data at baseline and follow-up. The exclusion criteria were (1) baseline WMH total score >1; (2) patients with history of brain trauma, neurological, or psychiatric diseases; and (3) abnormal brain MRI findings during follow-up (e.g., hemorrhage, infarction and other space-occupying lesions).

Ethics approval and consent to participate. All protocols performed in this study were reviewed and approved by the medical ethics committee of the Second Affiliated Hospital, Zhejiang University School of Medicine (No. 2013011 and 20230412) and adhered to the ethical principles expressed in the Declaration of Helsinki. All participants signed informed consent before enrollment.

Assessment of VRF score

Information on vascular risk factors was obtained at baseline. A composite vascular risk factor (VRF) score was calculated by summing four vascular risk factors (0 to 4, 4 is worst): hypertension, hypercholesterolemia, diabetes, ever smoker.[15] For hypertension, hypercholesterolemia, and diabetes, negative was defined as never having a formal diagnosis (based on self-report), positive was defined as having a formal diagnosis either currently or previously, regardless of medication status. Ever smoking was defined as being an active smoker or a past smoker.

Data acquisition

Both CSVD and NC participants underwent multimodal MRI by a 3.0 T MR (Discovery MR750, GE Healthcare, USA) scanner using an 8-channel brain phased array coil. The scanning sequences included 3 D-T1w imaging, T2 FLAIR imaging, diffusion tensor imaging (DTI), 3 D arterial spin labeling (ASL) imaging and susceptibility-weighted imaging (SWI). The 3 D-T1w image was acquired using spoiled gradient echo sequence with repetition time (TR) = 7.3 ms, echo time (TE) = 3.0 ms, inversion time = 450 ms, flip angle = 8°, slice thickness = 1 mm, matrix = 250×250, FOV = 25 cm × 25 cm. T2 FLAIR acquisition parameters were: TR/TE = 8400/150 ms, inversion time = 2100 ms, flip angle = 90°, FOV = 24 cm × 24 cm, matrix size = 256×256, slice thickness = 4.0 mm with no gap between slices. DTI was acquired with a single shot, diffusion-weighted spin-echo echo-planar imaging sequence. Thirty noncollinear directions were acquired with a b-value of 1000 s/mm^2. Five additional volumes were acquired without diffusion weighting (b-value = 0 s/mm^2). Other parameters of DTI were as follows: TR/TE = 8000/80.8 ms, flip angle = 90°, slice thickness = 2 mm without slice gap, isotropic voxel size = $2 \times 2 \times 2$ mm^3, matrix size = 128×128, FOV = 256 mm × 256 mm. The pulsed-continuous ASL data were acquired using a 3 D spiral readout fast spin-echo sequence with background suppression. The parameters were: TR/TE = 4611/10.5 ms, post label delay (PLD) = 1,525 ms, Label duration = 1500 ms, flip angle = 111°, slice thickness = 4 mm, matrix = 64×64, FOV = 24 cm. The SWI sequence was acquired in an axial orientation parallel to the anterior commissure to posterior commissure line, using a three-dimension multi-echo gradient-echo sequence (mGRE) with 8 equally spaced echoes: first echo time = 4.5 ms, echo spacing = 3.65 ms, last echo time = 30 ms, repetition time = 34 ms, FOV = 24 cm × 24 cm, matrix size = 416×384, flip angle = 20°, slice thickness = 2.0 mm with no gap between slices, and the in-plane spatial resolution interpolated into 0.4688 mm/pixel × 0.4688 mm/pixel. Magnitude and phase images were reconstructed and saved.

Image processing

Segmentation of white matter mask. The supratentorial white matter (WM) mask for each subject was generated from baseline T1 image using Sequence Adaptive Multimodal SEGmentation (SAMSEG) tool from FreeSurfer (https://surfer.nmr.mgh.harvard.edu/fswiki/Samseg/). Briefly, SAMSEG is an automated technique for whole-brain segmentation, capable of segmenting 41 anatomical structures from brain MRI images. This method uses a mesh-based computational atlas combined with a Gaussian appearance model, achieving high segmentation accuracy and reliability. We combined the segmented structures, including Left WM, Right WM and WMH, into a whole WM mask. The baseline WM masks were then eroded by 1 voxel and transformed to each follow-up T1 space for further analyses.

Segmentation of stable WMH and stable NAWM masks in CSVD. Figure 1(a) illustrates the pipeline of generation and registration of WM masks. Specifically, WMH at each time point were segmented using the FLAIR and T1 images. Here we used Lesion Segmentation Tool (LST, https://www.applied-statistics.de/lst/) in SPM 12 (Statistical Parametric Mapping, https://www.fil.ion.ucl.ac.uk/spm/), which has been widely used and proved to be a robust tool for longitudinal lesion quantification. We used the lesion prediction algorithm (LPA) and the longitudinal processing pipeline. Here, a with-in subject average T1 image was created and all WMH masks and images were automatically transformed to the cross-time template space (created by individual T1 images of all timepoints). All WMH masks were then manually modified to rectify any false lesion classifications (e.g., scalp and skull).

Following segmentation, the baseline WM mask (already eroded) was transformed to the cross-time template space. Subsequently, all time WMH masks were combined and dilated by 1 voxel, and this dilated mask was removed from WM mask to create stable normal-appearing WM (NAWM). The WMH (without dilation) present at all time points were classified as stable WMH (Figure 1(b)). After ROIs calculation, all masks in cross-time template space were restricted in WM and transformed to individual T1 space of each time point for further analyses.

We did not calculate the region of WMH growth, because of the difficulty in distinguishing such slow growth from the influence of partial volume effects (PVE). Moreover, our primary emphasis is the change in diffusion metrics. Besides, we did not calculate the WMH and NAWM ROIs in the NC group due to the small WMH volume. Usually, they only possessed punctate WMH, and it is very difficult to obtain robust and consistent segmentations across time points.

Calculation of CBF. After the acquisition, the scanner produced an averaged subtraction image (tag-control) and a proton density image for each subject. The images were transformed into NIFTI format and processed using Bayesian Inference for Arterial Spin Labeling MRI (BASIL, https://fsl.fmrib.ox.ac.uk/fsl/fslwiki/BASIL) and CAT12 (https://neuro-jena.github.io/cat/). The processing steps included: (1) Brain tissue
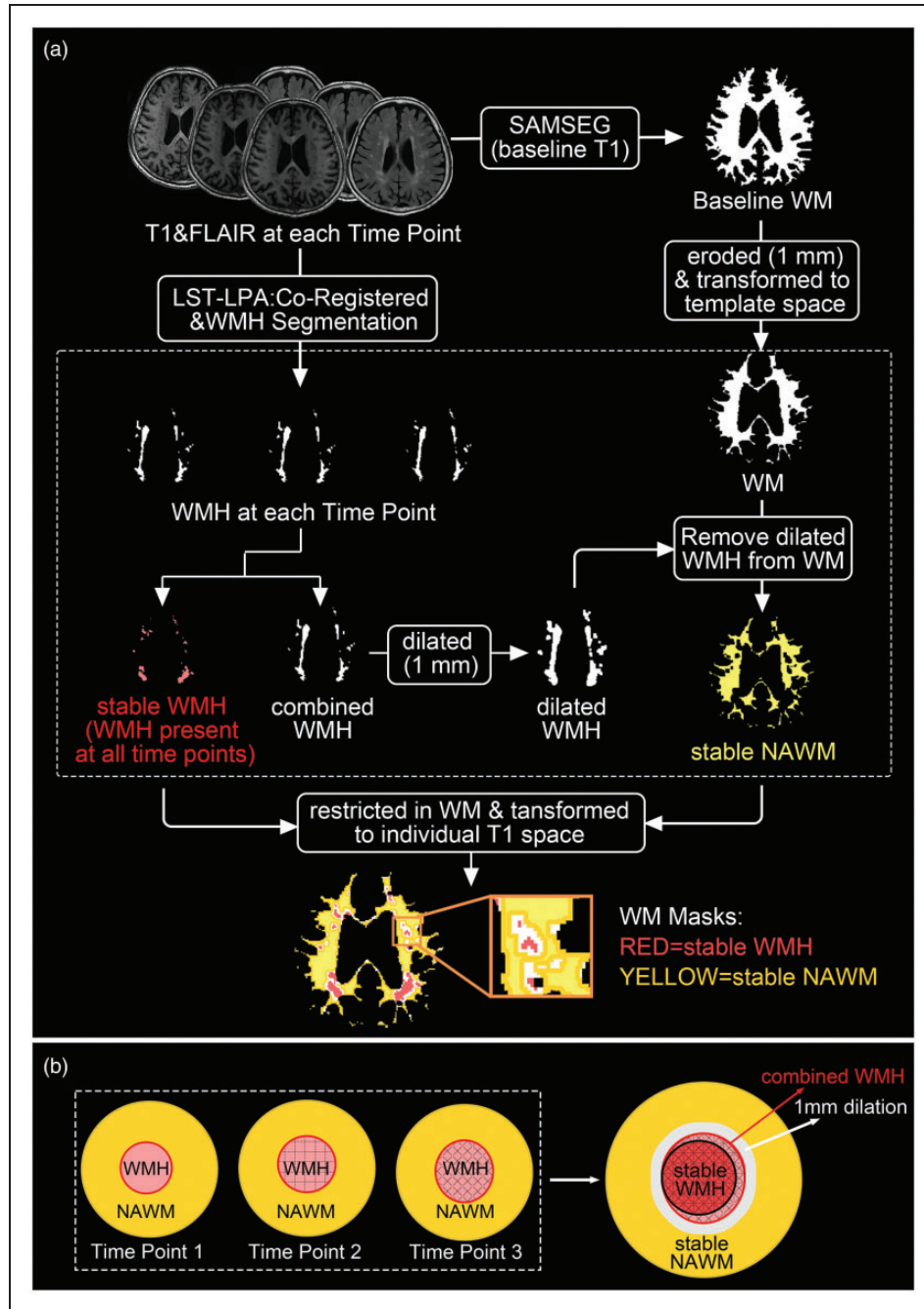
Figure 1. (a) Pipeline of generation and registration of WM masks in CSVD. WM masks within the dashed line were in the cross-time template space and (b) a schematic diagram of stable WMH and stable NAWM. LST: Lesion Segmentation Toolbox; LPA: lesion prediction algorithm; SAMSEG: Sequence Adaptive Multimodal SEGmentation; WM: white matter; WMH: white matter hyperintensities; NAWM: normal appearing WM.

segmentation using CAT12. We chose this method but not the built-in fsl_anat procedure because it had higher accuracy. (2) Registration of ASL images to structural images using the boundary-based registration (BBR) cost function. (3) Calibration using the proton density image and methods in a consensus article[16] to produce quantitative CBF maps. After these steps, the BASIL generated CBF maps in three spaces: native ASL space, native structural space, and standard space. The CBF images in the structural space were used to calculate mean CBF in WM, stable WMH, and stable NAWM.

Calculation of FW. Raw diffusion data were first preprocessed using FMRIB's Software Library (FSL, https://fsl.fmrib.ox.ac.uk/fsl/fslwiki/FSL/) and Advanced Normalization Tools (ANTs, https://picsl.upenn.edu/software/ants/), including signal denoising, Gibbs ringing removal, eddy-current and head motion correction, bias field correction, and brain masking. Visual quality control was performed to ensure the quality of the data preprocessing steps.

FW calculation was performed using the script provided by the MarkVCID project (https://markvcid.partners.org/markvcid2-protocols-resources). Briefly, the signal was fitted to a two-compartment model in each voxel, including a FW compartment (isotropic tensor) and a tissue compartment (anisotropic tensor). The FW map represents the fractional volume (ranging from 0 to 1) of the FW compartment. After calculation, the FW maps were then co-registered to T1 images through b0 images using Boundary-Based Registration (BBR, https://fsl.fmrib.ox.ac.uk/fsl/fslwiki/FLIRT_BBR). BBR is an advanced method to register EPI and structural images. By relying on intensities near the white matter boundary, BBR is likely to be more robust to various distortions and artifacts present in either the EPI or the structural image. Finally mean FW were extracted from the whole WM, stable WMH, and stable NAWM.

Calculation of total apparent fiber density. In the present study, we employed a quantitative measure for assessing WM microstructure, called apparent fiber density (AFD), which represents the relative amount of white matter fiber axons per unit volume of tissue[17] and had been previously adopted in many studies.[18,19] AFD is computed by fiber orientation distributions (FODs) using spherical deconvolution (CSD). Firstly, the 3-tissue response functions including WM, gray matter (GM), and cerebrospinal fluid (CSF) were directly estimated for each subject using the dwi2response dhollander algorithm in MRtrix3 (https://www.mrtrix.org/). Subsequently, the response functions obtained from all participants for each tissue type were averaged by group. Afterward, the preprocessed diffusion data were up-sampled, resulting in $1.25\,mm^3$ isotropic voxels. Then the WM fiber orientation distributions (FODs) for each subject were computed using the up-sampled diffusion data and the group averaged response function via single-shell 3-tissue CSD (SS3T-CSD) in MRtrix3Tissue (https://3tissue.github.io/). Next, the WM FODs further went through bias fields correction and global intensity normalization. Finally, the voxel-based AFD_t map (the total AFD summed over all orientations[20]) was obtained from the integral of WM FODs. The AFD_t map was co-registered to T1 images through b0 images, and mean AFD_t were extracted from the whole WM, stable WMH, and stable NAWM.

Assessment of SVD summary score. SVD markers, that is, WMH, PVS dilation, lacunes, and microbleeds at baseline, were visually assessed according to the Standards for Reporting Vascular Changes on Neuroimaging (STRIVE-1 and -2)[6,21] by an experienced neuroradiologist (ML). Lacunes were defined as a round or ovoid, subcortical, fluid-filled cavity (signal similar to CSF) with diameters ranging from 3 to 15 mm, consistent with a previous acute small subcortical infarct or hemorrhage in the territory of one perforating arteriole. Microbleeds were defined as small areas of signal void with associated blooming seen on SWI images. PVS evaluation was based on T1-weighted images, a method that has been previously adopted in many papers.[22,23] PVS score in basal ganglia was defined according to their numbers: degree 1, <5; degree 2, 5 and 10; degree 3, >10 but still numerable; and degree 4, when an innumerable number of PVS appeared in a cribriform change in basal ganglia.

The severity of SVD was assessed according to an ordinal summary SVD score[24] (ranging from 0 to 4) based on the information on lacunes, microbleeds, PVS, and Fazekas scale. One point was awarded for each of the following features: (1) presence of lacunes; (2) presence of microbleeds; (3) presence of PVS (defined as moderate to severe (grades 2–4) PVS in the basal ganglia); (4) presence of WMH (defined as either Fazekas score 2 or 3 for deep WMH; or Fazekas score 3 for periventricular WMH).

Statistical analyses

Statistical analyses were performed using SPSS (V.26.0 for Windows) and R (version 4.2.3). Statistical significance was set at a probability value of <0.05. Baseline characteristics were described as mean (SD) for normally distributed data, median (interquartile range) for skewed distributed data. To assess the differences in baseline characteristics between the two groups, we utilized Student's t-test, χ^2, or Mann-Whitney U test based on the data characteristics.

Group comparison of baseline values and longitudinal changes in FW. The comparison of baseline WM FW between two groups were performed by general linear model, controlling for age and sex. The comparison of baseline FW between stable WMH and stable NAWM in CSVD were performed by paired-t test.

To investigate WM FW changes over time, linear mixed-effects models (LMMs, lme4 R packages) were performed for each group. The model used FW at all time points as the dependent variable, with time

(time = 0 as the first scan) as the fixed effect, and included the estimation of both the random intercept and the random slope for time, accounting for variability between participants. The effect of time represented the average annualized change of FW.

To investigate the differences in change of WM FW between the two groups, we performed LMMs across CSVD and NC participants. FW was set as the dependent variable, with baseline age, sex, group (group = 0 as NC), time, interaction term age × time and group × time as fixed effects, and time as the random effects for each subject. The interaction term group × time determined the difference of FW change rate between groups. In the CSVD group, we also performed similar models for stable NAWM and stable WMH (with region = 0 as NAWM, region = 1 as WMH).

Cross-sectional and longitudinal associations of FW with VRF, CBF and AFD$_t$. Cross-sectionally, we used general linear model to investigate the association between FW and VRF score, controlling for age and sex, and we used Pearson's correlation to investigate the relationship between FW and CBF and AFD$_t$ in the whole WM, stable WMH, and stable NAWM. All the correlations were further analyzed using Pearson's partial correlation, controlling for age and sex.

To investigate which parameters can predict longitudinal FW elevation, LMMs were performed for each group respectively. Before prediction, WM FW were scaled across all time point scans (Z-scores) in each group, while VRF score, WM CBF and WM AFD$_t$ were scaled using baseline scans (Z-scores) in each group. The base model (model 1) used WM FW at each time point as the dependent variable, with baseline VRF score, baseline WM CBF, baseline WM AFD$_t$ and their interaction term with time as predictors, and baseline age, sex, age × time as covariates of no interest. A random intercept and a random slope of time for each subject were included. We then added baseline SVD summary score and its interaction term with time in the base model serving as additional covariates (model 2).

Correlations between FW and cognition in CSVD. We extracted individual slope values from LMMs on longitudinal WM FW and MoCA scores in CSVD respectively (with only time as a fixed effect), which represent the individual annual rate of WM FW and MoCA changes. Pearson's partial correlations were performed: between WM FW and MoCA scores at baseline, controlling for age, sex, and education; and between their slopes, controlling for age, sex, education, and total follow-up time.

Results

A total of 80 CSVD patients (224 scans in total, range: 2–4 scans) and 40 NC participants (89 scans in total, range: 2–3 scans) were included. The CSVD group had a higher mean age and more males than the NC group. Additionally, CSVD patients had higher rates of hypertension and ever-smoking, and a higher burden of CSVD imaging markers (Table 1). All participants had baseline and follow-up diffusion imaging data, but CBF was only calculated in 75 CSVD patients and in 33 NC participants due to the lack of ASL data.

Higher level and faster increase of WM FW in CSVD compared to NC

WM FW was significantly higher (0.234 vs 0.188, P < 0.001) in the CSVD group compared to the NC group (Figure 2(a)). Longitudinally, WM FW significantly increased over time in both groups (CSVD: Estimate = 0.007, P < 0.001; NC: Estimate = 0.004, P < 0.001, Figure 2(b) and (c)). The LMMs analyses across CSVD and NC groups showed a significant Age effect on WM FW (Age: Estimate = 0.001, P < 0.001), while the effect of Age × Time was not significant (Age × Time: Estimate = 0.00006, P = 0.340). The significant Group × Time effect indicated that WM FW increased faster in CSVD compared to NC (Group × Time: Estimate = 0.002, P = 0.041).

Higher level and faster increase of FW in stable WMH compared to stable NAWM

Within the CSVD group, FW was significantly higher in stable WMH compared to stable NAWM (0.427 vs 0.219, P < 0.001, Figure 2(d)). Longitudinally, FW significantly increased in both WMH and NAWM (stable WMH: Estimate = 0.018, P < 0.001; stable NAWM: Estimate = 0.005, P < 0.001, Figure 2(e) and (f)). The LMMs analyses showed that FW increased faster in stable WMH than in stable NAWM (Region × Time: Estimate = 0.012, p < 0.001).

Associations of FW with VRF, CBF and AFD$_t$ at baseline

Figure 3(a) shows the WM FW values corresponding to each VRF score in both groups, and WM FW was not associated with VRF score in either group (CSVD: Estimate = 0.004, P = 0.560; NC: Estimate = 0.001, P = 0.320). Correlation analyses show that WM FW was significantly correlated with WM AFD$_t$ in each of the CSVD and NC groups, but only correlated with WM CBF in the CSVD group. These correlations remained statistically significant after controlling for age and sex (Figure 3(b) and (c)). Within the CSVD

Table 1. Baseline demographic and clinical data for the subject groups.

	CSVD cohort n = 80	NC cohort n = 40	p
Demographic characteristics			
Age, y, mean (SD)	66.31 (8.60)	60.41 (6.59)	**<0.001**
Sex(female), n (%)	30 (38%)	27 (68%)	**0.002**
MoCA score, mean (SD)	21.94 (5.27)	–	–
Visit times, n, median (IQR)	3 (2–3)	2 (2–2)	**<0.001**
Total follow-up time, y, mean (SD)	2.75 (1.30)	2.62 (0.94)	0.580
Vascular risk factors (VRF)			
Hypertension, n (%)	57 (71%)	9 (23%)	**<0.001**
Diabetes, n (%)	15 (19%)	4 (10%)	0.166
Hyperlipemia, n (%)	11 (14%)	10 (25%)	0.103
Ever-smoking, n (%)	27 (34%)	3 (8%)	**0.001**
VRF score, median (IQR)	1 (1–2)	0 (0–1)	**<0.001**
Imaging characteristics			
WMH volume, ml, median (IQR)	10.46 (2.81–23.34)	0.81 (0.41–1.37)	**<0.001**
With lacunes, n (%)	60 (75%)	0 (0%)	**<0.001**
With microbleeds, n (%)	51 (64%)	0 (0%)	**<0.001**
bgPVS score, median (IQR)	3 (2–3)	2 (2–3)	**0.015**
SVD score, median (IQR)	3 (2–4)	1 (1–1)	**<0.001**

P values <0.05 are indicated in bold. CSVD: cerebral small vessel disease; NC: normal control; IQR: interquartile range; bgPVS: basal ganglia perivascular space; SVD score: small vessel disease score.
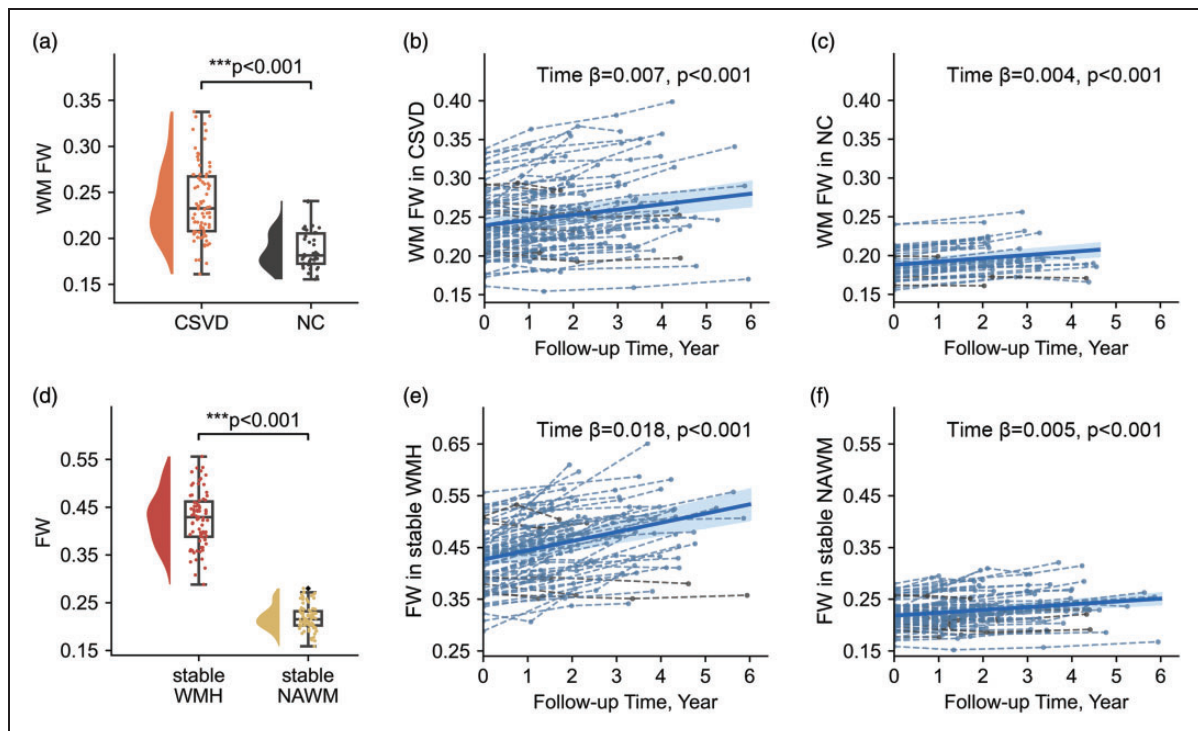

Figure 2. Comparison of baseline values and longitudinal changes in FW. (a) Comparison of baseline WM FW between CSVD and NC, controlling for age and sex. (b & c) WM FW trajectory over time in each group. (d) Comparison of baseline FW between WMH and NAWM by paired-t test and (e & f) FW trajectory over time in WMH and NAWM in the CSVD group. Dashed lines and spots represent WM FW changes at individual level, and the bold line represents the time-course estimated by the linear mixed-effects model at the group level. CSVD: cerebral small vessel disease; NC: normal control; FW: free water; WM: white matter. WMH: white matter hyperintensities; NAWM: normal appearing WM.
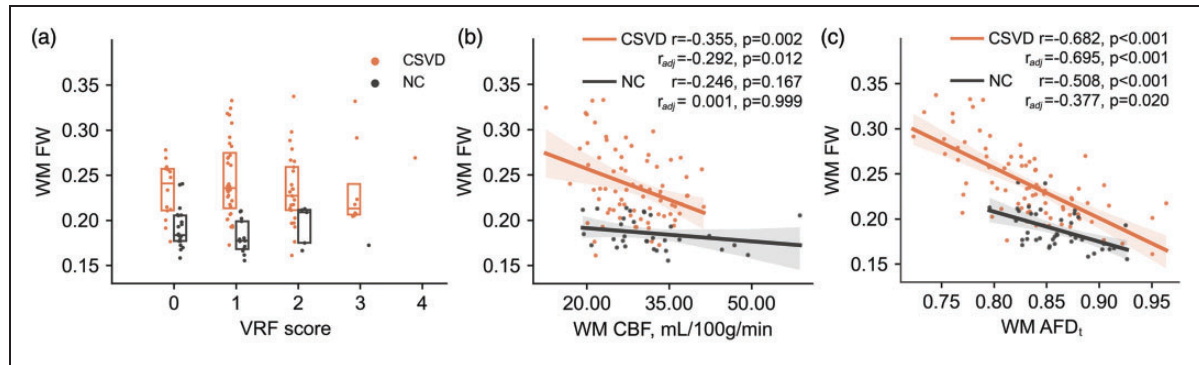
Figure 3. Associations of FW with VRF, CBF and AFD_t in WM. (a) WM FW values corresponding to each VRF score. (b) Correlation between FW and CBF and (c) correlation between FW and AFD_t. WM: white matter; CSVD: cerebral small vessel disease; NC: normal control; VRF: vascular risk factor; FW: free water; CBF: cerebral blood flow; AFD_t: total apparent fiber density.

Table 2. Fixed effects results for WM FW in the CSVD group.

Independent variables	Model 1		Model 2	
	Estimate (95% CI)	p	Estimate (95% CI)	p
Age	0.027 (0.013, 0.041)	<0.001	0.021 (0.009, 0.034)	0.001
Age × Time	0.000 (−0.003, 0.003)	0.820	0.000 (−0.003, 0.003)	0.977
Sex	−0.101 (−0.365, 0.163)	0.456	−0.100 (−0.330, 0.129)	0.394
Time	0.111 (−0.079, 0.302)	0.258	0.089 (−0.105, 0.283)	0.372
VRF score Zsc	−0.088 (−0.224, 0.049)	0.213	−0.121 (−0.237, −0.005)	0.044
VRF score Zsc × Time	−0.001 (−0.027, 0.025)	0.922	−0.003 (−0.029, 0.023)	0.822
WM CBF Zsc	−0.158 (−0.294, −0.023)	0.025	−0.047 (−0.168, 0.074)	0.450
WM CBF Zsc × Time	−0.008 (−0.034, 0.018)	0.565	−0.002 (−0.029, 0.025)	0.891
WM AFD_t Zsc	−0.549 (−0.681, −0.418)	<0.001	−0.493 (−0.605, −0.380)	<0.001
WM AFD_t Zsc × Time	−0.034 (−0.058, −0.009)	**0.010**	−0.031 (−0.056, −0.007)	**0.017**
SVD score	–	–	0.300 (0.194, 0.405)	<0.001
SVD score × Time	–	–	0.015 (−0.008, 0.039)	0.212

Interaction terms in bold italic represent whether a specific factor could predict the progression of FW. P values <0.05 are indicated in bold. Zsc is short of Z score. WM: white matter; VRF: vascular risk factor; CBF: cerebral blood flow; AFD_t: total apparent fiber density; SVD score: small vessel disease score.

group (Supplementary Information, Fig. S1), FW was significantly correlated with CBF and AFD_t in both WMH and NAWM (CBF: WMH, r = −0.287, P = 0.013, NAWM, r = −0.277, P = 0.017; AFD_t: WMH, r = −0.573, P < 0.001, NAWM, r = −0.645, P < 0.001), but only the correlations with AFD_t remained statistically significant (r_{adj} = −0.649, P < 0.001) after controlling for age and sex.

Effect of baseline VRF, CBF and AFD_t on FW elevation over time

Higher baseline WM AFD_t predicted a slower WM FW elevation over time in the CSVD group (WM AFD_t Zsc × Time: Estimate = −0.034, P = 0.010; Table 2, model 1), and the effect remained significant, after adding SVD score × Time (Table 2, model 2).

Neither baseline VRF score, nor WM CBF was associated with WM FW elevation over time. For the NC group, higher baseline WM CBF predicted a slower WM FW elevation over time (WM CBF Zsc × Time: Estimate = −0.054, P = 0.019, Table 3, model 1), and the effect remained significant, after adding SVD score × Time (Table 3, model 2). No significant effects of baseline VRF score or WM AFD_t on WM FW elevation over time was found.

When analyzing WMH and NAWM separately, higher baseline AFD_t predicted a slower FW elevation over time in both stable WMH (WMH AFD_t Zsc × Time: Estimate = −0.053, P = 0.016, Supplementary Information, Table S1, model 1) and stable NAWM (NAWM AFD_t Zsc × Time: Estimate = −0.036, P = 0.047, Table S2, model 1). After adding SVD score × Time, the effect remained significant in stable

Table 3. Fixed effects results for WM FW in the NC group.

Independent variables	Model 1		Model 2	
	Estimate (95% CI)	p	Estimate (95% CI)	p
Age	0.043 (0.004, 0.082)	0.037	0.041 (0.002, 0.080)	0.048
Age × Time	0.001 (−0.005, 0.006)	0.829	0.001 (−0.005, 0.006)	0.802
Sex	0.324 (−0.159, 0.807)	0.198	0.298 (−0.188, 0.784)	0.239
Time	0.155 (−0.175, 0.486)	0.364	0.16 (−0.186, 0.506)	0.372
VRF score Zsc	−0.060 (−0.289, 0.169)	0.610	−0.06 (−0.287, 0.167)	0.610
VRF score Zsc × Time	−0.021 (−0.058, 0.017)	0.287	−0.021 (−0.058, 0.017)	0.285
WM CBF Zsc	0.084 (−0.185, 0.352)	0.545	0.083 (−0.184, 0.349)	0.546
WM CBF Zsc × Time	−0.054 (−0.098, −0.011)	**0.019**	−0.055 (−0.098, −0.011)	**0.019**
WM AFD$_t$ Zsc	−0.308 (−0.536, −0.079)	0.013	−0.318 (−0.547, −0.089)	0.010
WM AFD$_t$ Zsc × Time	−0.029 (−0.061, 0.003)	0.089	−0.029 (−0.061, 0.004)	0.096
SVD score	–	–	0.293 (−0.599, 1.186)	0.524
SVD score × Time	–	–	−0.012 (−0.160, 0.137)	0.880

Interaction terms in bold italic represent whether a specific factor could predict the progression of FW. P values <0.05 are indicated in bold. Zsc is short of Z score. WM: white matter; VRF: vascular risk factor; CBF: cerebral blood flow; AFD$_t$: total apparent fiber density; SVD score: small vessel disease score.
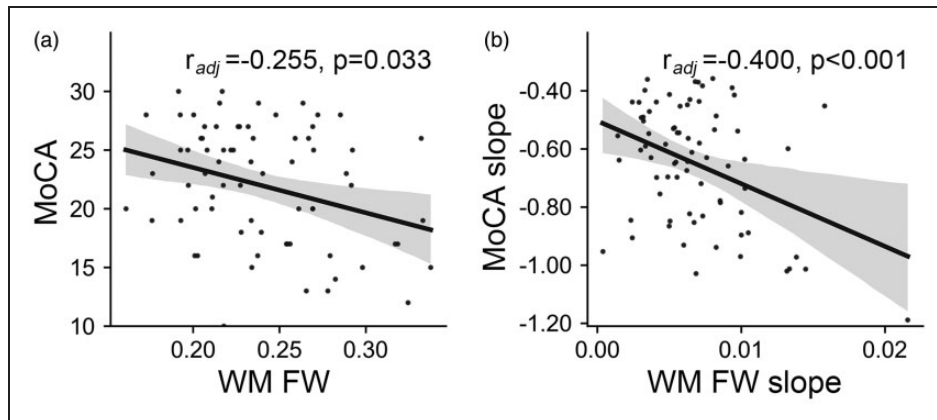

Figure 4. Cross-sectional and longitudinal correlations between FW and MoCA in CSVD. (a) Correlation between WM FW and MoCA at baseline and (b) correlation between WM FW slope and MoCA slope. The slope represents the annual rate of change. WM: white matter; FW: free water; MoCA: Montreal Cognitive Assessment.

WMH but became nonsignificant in stable NAWM (Supplementary Information, Table S1, model 2, Table S2, model 2). No significant effects of VRF score × Time or CBF × Time were observed in stable WMH or in stable NAWM.

Cross-sectional and longitudinal correlations between FW and cognition in CSVD

At baseline, WM FW was significantly correlated with MoCA scores, controlling for age, sex and education ($r_{adj} = -0.255$, $p = 0.033$, Figure 4(a)). longitudinally, faster WM FW elevation was significantly correlated with faster MoCA score decline over time, controlling for age, sex, education and total follow-up time ($r_{adj} = -0.400$, $P < 0.001$, Figure 4(b)).

Discussion

In the current study, we found that FW was higher at baseline and increased more rapidly in CSVD patients than in NC participants. When investigating WMH and NAWM separately in CSVD patients, FW was higher at baseline and increased more rapidly in WMH than in NAWM. In both patients and controls, WM AFD$_t$ was negatively associated with FW at baseline, but lower baseline WM AFD$_t$ could only predict the longitudinal elevation of FW in CSVD patients. In the NC group, WM CBF could predict the longitudinal elevation of WM FW. In the CSVD group, WM FW was associated with MoCA at baseline, and the slope of FW change was associated with the slope of MoCA change.

Previous studies have demonstrated a tight association between CSVD and FW.[11,12,25] Nonetheless, longitudinal analyses, which are crucial for understanding the specific contribution of CSVD to FW, are scarce. A recent study based on CSVD patients (N = 51) did not find FW elevation in WMH and NAWM regions over 1–2 years, which might be due to the small sample size and relatively lighter disease burden (WMH volume: 5.3 ± 7.2 ml).[26] Indeed, we observed a significant age effect on FW value although not on longitudinal FW elevation, might due to the short follow-up intervals. Even in the NC group, we found significant FW elevation at follow-ups. These results indicate that aging-related brain degeneration alone could cause increased FW. Nevertheless, FW elevated nearly two-times faster (Estimates: 0.007 vs. 0.004) in CSVD patients, confirming the additional impact of CSVD.

Notably, longitudinal FW elevations in WMH lesions were more than triple (Estimates: 0.018 vs. 0.005) of those in NAWM. This indicates that the accumulation of FW was not homogeneous across the whole brain, but mainly occurred in WMH regions. It seems that pathological changes within WMH had a greater influence on FW than global factors. Previous pathological studies have demonstrated a variety of changes in WMH, including blood-brain barrier disruption, vacuolation, tissue rarefaction, vasogenic edema, etc.[27–29] These pathological changes can directly cause the increase of interstitial fluid. The fact that FW increase in the NAWM of CSVD is close to FW increase in the WM of NC (0.005 vs. 0.004) also suggest a trivial contribution of global pathological factors.

In the CSVD group, a lower AFD_t was independently associated with a faster increase in FW over time. WM fiber alterations, primarily characterized by demyelination, axonal loss, and reduced density of oligodendrocytes,[27] could lead to the dilation of extracellular spaces, where fluid can readily accumulate. Myelin vacuolation, a result of myelin degeneration,[30] may allow for unrestricted water molecule movement within the cavity and increase FW fraction.[31] Severe WM fiber alterations is commonly accompanied by other pathological mechanisms such as neuroinflammation, leading to further elevation on FW.[32,33] Moreover, focal WM lesions could lead to degeneration in the remote part of the crossing fiber tract, further accelerating FW elevation over time. Compared to in NAWM, these pathologies are more pronounced in WMH, therefore AFD_t had more contribution to FW increase (Supplementary Information, Table S1). In the NAWM of the CSVD group and the whole WM of the NC group, the effect of AFD_t was nonsignificant, although trends were observed (P = 0.060 and 0.096, respectively).

A lower WM CBF was only associated with a faster increase of WM FW in the NC but not the CSVD group. Besides, VRF score was not associated with WM FW change in either group. These results seem contradictory to previous conceptions regarding the association between FW and vascular pathology. Nonetheless, it should be noted that previous studies regarding whether CBF could predict CSVD progression also showed conflicting results. A 4-year follow-up study, included 575 CSVD patients, reported that baseline global CBF was not associated with WMH progression.[34] Another large study (N = 390) demonstrated that a decline in global CBF over 2.75 years was associated with a progression in periventricular WMH but not in deep WMH.[35] The high inter-subject variability of CBF might contribute to the inconsistent results. It has been shown that aging, arterial oxygenation, and some vasoconstrictive/vasodilatory substances could influence CBF.[36,37] In CSVD, white matter lesions can also cause tissue degeneration in remote brain regions,[38,39] leading to CBF reduction. It is difficult to control all these factors and some negative results might have been caused by these confounders. It is also possible that the VRFs and CBF are upstream factors, and FW, a parenchymal marker, might be more associated with direct parenchymal pathologies but not upstream vascular pathologies. Therefore, a larger sample size and a longer follow-up duration may be needed for detecting the small effect size.

In correlation with cognition, we found that higher WM FW was associated with cognitive impairment (assessed by MoCA) in the CSVD group, and faster FW elevation might accelerate cognitive decline. Similarly, Ottoy et al.[40] found in a cross-sectional study that FW value in WMH or NAWM associated with cognitive impairment in patients with Alzheimer's disease, and Maillard et al.[12] found that longitudinal changes in FW associated with cognitive decline in non-demented community people. Our findings support the notion that WM FW is a sensitive marker of cognition, and monitoring FW accumulation in WM may help predict the cognitive impairment process.

The current study had several limitations. First, the two cohorts of CSVD and NC had significant differences in age and sex. While we adjusted them in all analyses, potential non-linear effect might still influence the results. Second, the study was based on an East Asian population from a single site, so that our findings may be not generalizable to other populations. Future research should include more diverse populations from multiple sites to enhance the generalizability of our results. Third, using single-shell diffusion data for the calculation of FW and AFD_t could introduce some inaccuracies. Due to the long scanning time, multi-shell diffusion data is relatively scarce in previous

clinical imaging studies. Future studies using accelerated imaging method may overcome this limitation. Nonetheless, previous studies demonstrated that these diffusion parameters calculated using single-shell diffusion data were well-correlated with disease severity and clinical functions,[11,12,18,40,41] suggesting their usefulness in clinical studies. Fourth, we used CBF derived from ASL with a short PLD for all participants. Ideally, a longer PLD should be applied due to the delayed transit time. Nonetheless, previously we found that the correlation between CBFs derived from short and long PLDs were very high (>0.9), so the potential bias should be small.[42] Fifth, we had not assessed the contribution of other potential pathological mechanisms, such as blood-brain barrier (BBB) disruption. Verifying the contribution of BBB would require dynamic contrast-enhanced imaging which is relatively difficult to be implemented in community participants. Sixth, this was a retrospective study and the patients had different numbers of scans and follow-up times. This might cause differences in the weightings of individual patients and induce additional variance. Finally, in our study, treatments for vascular risk factors and prevention of stroke were not accounted, since variations in patients' medication and risk factor control could lead to over 20 subgroups with too few participants for subgroup analysis, and the span of follow-up times and irregular medication adherence might not accurately reflect the impact of actual treatment.

Despite these limitations, the strengths of this study include the longitudinal cohorts with both CSVD and community participants, multiple diffusion MRI data collected from an identical scanner, and careful adjustments for potential covariates. The contribution of CSVD to FW was confirmed by a higher FW elevation rate in the CSVD group, which could be predicted by baseline CSVD-related factors. The result from subregion analyses further indicate that WMH-related local pathologies are likely to be a major contributor to FW elevation. These findings could provide support for future observational or interventional studies utilizing FW to reflect CSVD progression.

Conclusions

CSVD is associated with a faster increase in WM FW, which was mainly driven by FW increase in WMH region. WM fiber alterations and hypoperfusion might accelerate WM FW elevation over time. WM FW elevation is associated with cognitive decline.

Data availability

Data will be made available on request.

Declaration of conflicting interests

The author(s) declared no potential conflicts of interest with respect to the research, authorship, and/or publication of this article.

Authors' contributions

ML analyzed the data. ML, RZ, PH interpreted the data and drafted the manuscript. LX, YZ, HH, LC, SW, LL, ML, YJ, XY and PH contributed to the data acquisition. PH, RZ, and MZ designed of the study, and the set-up of the subject scan protocol, supervised the work. PH, RZ, and AL revised the manuscript. All authors have read and approved the final manuscript for publication.

Supplemental material

Supplemental material for this article is available online.

ORCID iDs

Minming Zhang https://orcid.org/0000-0003-2084-203X
Peiyu Huang https://orcid.org/0000-0003-0145-7558

References

1. Wardlaw JM, Smith C and Dichgans M. Small vessel disease: mechanisms and clinical implications. *Lancet Neurol* 2019; 18: 684–696.
2. Wilcock D, Jicha G, Blacker D, et al. MarkVCID cerebral small vessel consortium: I. Enrollment, clinical, fluid protocols. *Alzheimers Dement* 2021; 17: 704–715.
3. Lu H, Kashani AH, Arfanakis K, et al. MarkVCID cerebral small vessel consortium: II. Neuroimaging protocols. *Alzheimers Dement* 2021; 17: 716–725.
4. Markus HS, Van Der Flier WM, Smith EE, et al. Framework for clinical trials in cerebral small vessel disease (FINESSE): a review. *JAMA Neurol* 2022; 79: 1187–1198.
5. Smith EE, Biessels GJ, De Guio F, et al. Harmonizing brain magnetic resonance imaging methods for vascular contributions to neurodegeneration. *Alzheimers Dement (Amst)* 2019; 11: 191–204.
6. Duering M, Biessels GJ, Brodtmann A, et al. Neuroimaging standards for research into small vessel disease – advances since 2013. *Lancet Neurol* 2023; 22: 602–618.

7. Maillard P, Lu H, Arfanakis K, et al. Instrumental validation of free water, peak-width of skeletonized mean diffusivity, and white matter hyperintensities: MarkVCID neuroimaging kits. *Alzheimer's Dement Diagnosis, Assess Dis Monit* 2022; 14: e12261.

8. Pasternak O, Sochen N, Gur Y, et al. Free water elimination and mapping from diffusion MRI. *Magn Reson Med* 2009; 62: 717–730.

9. Maillard P, Mitchell GF, Himali JJ, et al. Aortic stiffness, increased white matter free water, and altered microstructural integrity: a continuum of injury. *Stroke* 2017; 48: 1567–1573.

10. Petrea RE, Pinheiro A, Demissie S, et al. Hypertension trends and white matter brain injury in the offspring Framingham heart study cohorts. *Hypertension* 2024; 81: 87–95.

11. Huang P, Zhang R, Jiaerken Y, et al. White matter free water is a composite marker of cerebral small vessel degeneration. *Transl Stroke Res* 2022; 13: 56–64.

12. Maillard P, Fletcher E, Singh B, et al. Cerebral white matter free water: a sensitive biomarker of cognition and function. *Neurology* 2019; 92: E2221–E2231.

13. Archer DB, Moore EE, Shashikumar N, et al. Free-water metrics in medial temporal lobe white matter tract projections relate to longitudinal cognitive decline. *Neurobiol Aging* 2020; 94: 15–23.

14. Fazekas F, Chawluk JB, Alavi A, et al. MR signal abnormalities at 1.5 T in Alzheimer's dementia and normal aging. *AJR Am J Roentgenol* 1987; 149: 351–356.

15. Cai M, Jacob MA, Van Loenen MR, et al. Determinants and temporal dynamics of cerebral small vessel disease: 14-year follow-up. *Stroke* 2022; 53: 2789–2798.

16. Alsop DC, Detre JA, Golay X, et al. Recommended implementation of arterial spin-labeled perfusion MRI for clinical applications: a consensus of the ISMRM perfusion study group and the European consortium for ASL in dementia. *Magn Reson Med* 2015; 73: 102–116.

17. Raffelt D, Tournier JD, Rose S, et al. Apparent fibre density: a novel measure for the analysis of diffusion-weighted magnetic resonance images. *Neuroimage* 2012; 59: 3976–3994.

18. Yu X, Yin X, Hong H, et al. Increased extracellular fluid is associated with white matter fiber degeneration in CADASIL: in vivo evidence from diffusion magnetic resonance imaging. *Fluids Barriers CNS* 2021; 18: 29–13.

19. Dewenter A, Jacob MA, Cai M, et al. Disentangling the effects of Alzheimer's and small vessel disease on white matter fibre tracts. *Brain* 2023; 146: 678–689.

20. Calamante F, Smith RE, Tournier JD, et al. Quantification of voxel-wise total fibre density: investigating the problems associated with track-count mapping. *Neuroimage* 2015; 117: 284–293.

21. Wardlaw JM, Smith EE, Biessels GJ, et al. Neuroimaging standards for research into small vessel disease and its contribution to ageing and neurodegeneration. *Lancet Neurol* 2013; 12: 822–838.

22. Gertje EC, van Westen D, Panizo C, et al. Association of enlarged perivascular spaces and measures of small vessel and Alzheimer disease. *Neurology* 2021; 96: e193–e202.

23. Zeng Q, Li K, Luo X, et al. The association of enlarged perivascular space with microglia-related inflammation and Alzheimer's pathology in cognitively normal elderly. *Neurobiol Dis* 2022; 170: 105755.

24. Staals J, Makin SDJ, Doubal FN, et al. Stroke subtype, vascular risk factors, and total MRI brain small-vessel disease burden. *Neurology* 2014; 83: 1228–1234.

25. Mayer C, Nägele FL, Petersen M, et al. Free-water diffusion MRI detects structural alterations surrounding white matter hyperintensities in the early stage of cerebral small vessel disease. *J Cereb Blood Flow Metab* 2022; 42: 1707–1718.

26. Sun Y, Hu Y, Qiu Y, et al. Characterization of white matter over 1–2 years in small vessel disease using MR-based quantitative susceptibility mapping and free-water mapping. *Front Aging Neurosci* 2022; 14: 998051.

27. Wardlaw JM, Valdés Hernández MC and Muñoz-Maniega S. What are white matter hyperintensities made of? Relevance to vascular cognitive impairment. *J Am Heart Assoc* 2015; 4: 001140.

28. Pettersen JA, Keith J, Gao F, et al. CADASIL accelerated by acute hypotension: arterial and venous contribution to leukoaraiosis. *Neurology* 2017; 88: 1077–1080.

29. Rudilosso S, Stringer MS, Thrippleton M, et al. Blood-brain barrier leakage hotspots collocating with brain lesions due to sporadic and monogenic small vessel disease. *J Cereb Blood Flow Metab* 2023; 43: 1490–1502.

30. Gouw AA, Seewann A, Van Der Flier WM, et al. Heterogeneity of small vessel disease: a systematic review of MRI and histopathology correlations. *J Neurol Neurosurg Psychiatry* 2011; 82: 126–135.

31. Duering M, Finsterwalder S, Baykara E, et al. Free water determines diffusion alterations and clinical status in cerebral small vessel disease. *Alzheimer's Dement* 2018; 14: 764–774.

32. Low A, Mak E, Rowe JB, et al. Inflammation and cerebral small vessel disease: a systematic review. *Ageing Res Rev* 2019; 53: 100916.

33. Di Biase MA, Zalesky A, Cetin-Karayumak S, et al. Large-scale evidence for an association between peripheral inflammation and white matter free water in schizophrenia and healthy individuals. *Schizophr Bull* 2021; 47: 542–551.

34. Ten Dam VH, Van Den Heuvel DMJ, De Craen AJM, et al. Decline in total cerebral blood flow is linked with increase in periventricular but not deep white matter hyperintensities. *Radiology* 2007; 243: 198–203.

35. Van Der Veen PH, Muller M, Vincken KL, et al. Longitudinal relationship between cerebral small-vessel disease and cerebral blood flow. *Stroke* 2015; 46: 1233–1238.

36. Claassen JAHR, Thijssen DHJ, Panerai RB, et al. Regulation of cerebral blood flow in humans: physiology and clinical implications of autoregulation. *Physiol Rev* 2021; 101: 1487–1559.

37. Marchal G, Rioux P, Sette G, et al. Regional cerebral oxygen consumption, blood flow, and blood volume in healthy human aging. *Arch Neurol* 1992; 49: 1013–1020.

38. Egorova N, Dhollander T, Khlif MS, et al. Pervasive white matter fiber degeneration in ischemic stroke. *Stroke* 2020; 51: 1507–1513.

39. Liu Y, Xia Y, Wang X, et al. White matter hyperintensities induce distal deficits in the connected fibers. *Hum Brain Mapp* 2021; 42: 1910–1919.

40. Ottoy J, Ozzoude M, Zukotynski K, et al. Amyloid-PET of the white matter: relationship to free water, fiber integrity, and cognition in patients with dementia and small vessel disease. *J Cereb Blood Flow Metab* 2023; 43: 921–936.

41. Jaroszynski C, Attyé A, Job A, et al. Tracking white-matter brain modifications in chronic non-bothersome acoustic trauma tinnitus. *NeuroImage Clin* 2021; 31: 102696.

42. Zhang R, Huang P, Wang S, et al. Decreased cerebral blood flow and delayed arterial transit are independently associated with white matter hyperintensity. *Front Aging Neurosci* 2022; 14: 762745–762748.